This article was downloaded by:
On: *23 January 2011*
Access details: *Access Details: Free Access*
Publisher *Taylor & Francis*
Informa Ltd Registered in England and Wales Registered Number: 1072954 Registered office: Mortimer House, 37-41 Mortimer Street, London W1T 3JH, UK

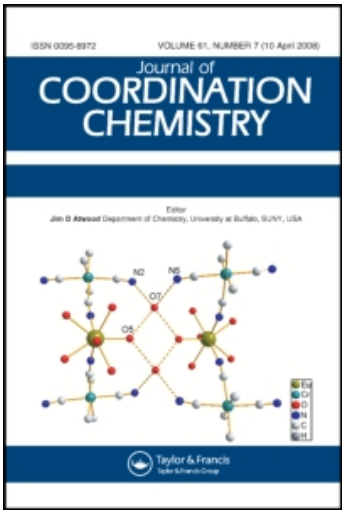


**Journal of Coordination Chemistry**
Publication details, including instructions for authors and subscription information:
http://www.informaworld.com/smpp/title~content=t713455674

# Thermodynamics and electrochemistry of manganese *ortho*-tetrakis(*N*-*n*-butylpyridinium-2-yl)porphyrin in aqueous solutions

Ana Budimir[a]; Tomislav Šmuc[a]; Tin Weitner[a]; Ines Batinić-Haberle[b]; Mladen Biruš[a]
[a] Faculty of Pharmacy and Biochemistry, University of Zagreb, Zagreb 10000, Croatia [b] Department of Radiation Oncology, Duke University Medical School, Durham, NC 27710, USA

First published on: 16 July 2010

**To cite this Article** Budimir, Ana , Šmuc, Tomislav , Weitner, Tin , Batinić-Haberle, Ines and Biruš, Mladen(2010) 'Thermodynamics and electrochemistry of manganese *ortho*-tetrakis(*N*-*n*-butylpyridinium-2-yl)porphyrin in aqueous solutions', Journal of Coordination Chemistry, 63: 14, 2750 — 2765, First published on: 16 July 2010 (iFirst)
**To link to this Article: DOI:** 10.1080/00958972.2010.502571
**URL:** http://dx.doi.org/10.1080/00958972.2010.502571

PLEASE SCROLL DOWN FOR ARTICLE

Full terms and conditions of use: http://www.informaworld.com/terms-and-conditions-of-access.pdf

This article may be used for research, teaching and private study purposes. Any substantial or systematic reproduction, re-distribution, re-selling, loan or sub-licensing, systematic supply or distribution in any form to anyone is expressly forbidden.

The publisher does not give any warranty express or implied or make any representation that the contents will be complete or accurate or up to date. The accuracy of any instructions, formulae and drug doses should be independently verified with primary sources. The publisher shall not be liable for any loss, actions, claims, proceedings, demand or costs or damages whatsoever or howsoever caused arising directly or indirectly in connection with or arising out of the use of this material.

*Journal of Coordination Chemistry*
Vol. 63, Nos. 14–16, 20 July–20 August 2010, 2750–2765

Taylor & Francis
Taylor & Francis Group

# Thermodynamics and electrochemistry of manganese *ortho*-tetrakis(*N*-*n*-butylpyridinium-2-yl)porphyrin in aqueous solutions

ANA BUDIMIR†, TOMISLAV ŠMUC†, TIN WEITNER†, INES BATINIĆ-HABERLE‡ and MLADEN BIRUŠ*†

†Faculty of Pharmacy and Biochemistry, University of Zagreb, A. Kovačića 1, Zagreb 10000, Croatia
‡Department of Radiation Oncology, Duke University Medical School, Durham, NC 27710, USA

Downloaded At: 07:10 23 January 2011

(*Received 2 February 2010; in final form 1 April 2010*)

Spectrophotometric pH-titrations ($1 < pH < 12$) of manganese *ortho*-tetrakis(*N*-*n*-butylpyridinium-2-yl)porphyrin (MnTnBu-2-PyP) have been performed in aqueous solution at various temperatures and ionic strengths, studying complexes of various manganese oxidation states (Mn(II)–(IV)). The observed results indicate three absorbing species of $Mn^{III}$TnBu-2-PyP, but only two absorbing species of $Mn^{II}$TnBu-2-PyP and $Mn^{IV}$TnBu-2-PyP within the studied acidity range. The first and second deprotonation constants are related to fully protonated and monodeprotonated species, i.e., the aqua and hydroxo complexes, respectively. The same complexes have been studied by cyclic-voltammetry and the results can be summarized as follows: $E^{0'}(Mn^{III}TnBu\text{-}2\text{-}PyP(H_2O)_2^{5+}/Mn^{II}TnBu\text{-}2\text{-}PyP(H_2O)^{4+}) = +0.203\,V$, $E^{0'}(Mn^{III}TnBu\text{-}2\text{-}PyP(H_2O)(OH)^{4+}/Mn^{II}TnBu\text{-}2\text{-}PyP(OH)^{3+}) = +0.191\,V$, and $E^{0'}(Mn^{IV}TnBu\text{-}2\text{-}PyP(H_2O)(OH)^{5+}/Mn^{III}TnBu\text{-}2\text{-}PyP(H_2O)_2^{5+}) = +0.62\,V$, all *versus* NHE. In neutral and acidic media the oxidation of the aqua Mn(III) complex may also occur as a one-electron two-proton process yielding the oxoaqua Mn(IV) complex.

*Keywords*: Manganese tetra(*ortho*-*n*-butylpyridyl)porphyrin; Thermodynamics; Electrochemistry; Ionic strength; Proton dissociation

## 1. Introduction

Metalloporphyrins have been utilized as important electron carriers in a variety of biological and chemical redox systems, as their electron-transfer reactions can be finely tuned by the metal, the porphyrin macrocycle, and the electronic properties of the axial ligands. Over the last decade, there has been a great deal of interest in manganese porphyrins (MnP) because of their high reactivity and the accessibility of several

*Corresponding author. Email: birus@pharma.hr


ISSN 0095-8972 print/ISSN 1029-0389 online © 2010 Taylor & Francis
DOI: 10.1080/00958972.2010.502571

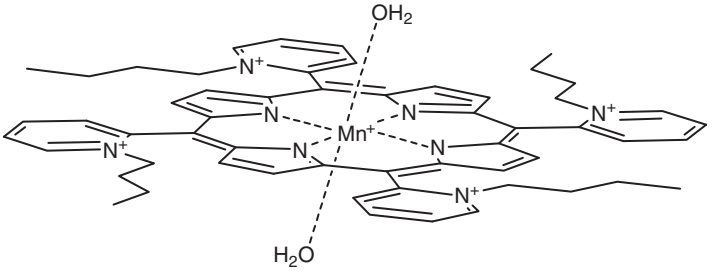


Figure 1. Manganese *ortho*-tetrakis(*N*-*n*-butylpyridinium-2-yl)porphyrin ($Mn^{III}$TnBu-2-PyP).

Downloaded At: 07:10 23 January 2011

oxidation states that enables the construction of redox cycles involving the consumption of superoxide and NO-derived oxidants at the expense of readily available biochemical reductants. There is a growing interest in using MnPs as therapeutics for oxidative stress-related diseases, as the removal of reactive oxygen and nitrogen species is redox-based [1–3]. A structure–activity relationship found for the manganese-centered reduction potential and the Mn-porphyrins catalytic rate constant of $O_2^{\bullet -}$ dismutation, guided the synthesis of the most potent functional superoxide dismutase (SOD)-mimics [4–8]. Modulation of SOD activity has been achieved by tuning the metal-centered reduction potential of metalloporphyrins *via* alkylation of the tetrapyridylporphyrin ring. Manganese *ortho*-tetrakis(*N*-ethylpyridinium-2-yl)porphyrin was found to have an excellent *in vitro* and *in vivo* SOD-like activity [7–9] and to exert an exceptional efficacy in ameliorating neurological disorders, injuries of central nervous system (stroke and spinal cord), radiation injury, cancer, diabetes, sickle cell disease, renal and cardiac ischemia reperfusion, and pain. In addition to the intrinsic antioxidant capacity of manganese porphyrins, bioavailability plays a major role in their *in vivo* efficacy [10]. For instance, the hexyl-MnP analogue (MnTnHex-2-PyP) exhibits similar antioxidant capacity as the ethyl-analogue (MnTE-2-PyP), but because of its higher lipophilicity the former is up to 120-fold more efficient in reducing oxidative stress injuries [11].

Among the manganese porphyrins where lipophilicity and the catalytic rate constant for $O_2^{\bullet -}$ dismutation were determined, *ortho*-tetrakis(*N*-*n*-butylpyridinium-2-yl)porphyrin (MnTnBu-2-PyP, figure 1) exhibits the antioxidant efficiency comparable to the most efficient methyl- and ethyl-analogues, while its partition between *n*-octanol and water (log $P_{OW}$) is *ca* 2 and 3 units more positive than the partition of other two analogues. Its lipophilicity that results in a high intracellular accumulation, along with its antioxidant potency, makes it prospective drug for treating diseases that have oxidative stress in common. The still relatively high hydrophilicity is expected to prevent its precipitation in strongly alkaline water solution, where the charge of the aqua complex reduces by two units due to the deprotonation of coordinated water. The latter property should allow a detailed study of both the proton-dependent speciation and the formal reduction potentials within a wide range of acidity, which should improve our understanding of *in vitro* and possibly *in vivo* catalytic effectiveness of manganese porphyrins.

In this work we present the results of spectrophotometric and voltammetric investigations of the deprotonation of MnTnBu-2-PyP at various temperatures and

ionic strengths of aqueous solutions for the Mn(II), Mn(III), and Mn(IV) porphyrin complexes.

## 2. Experimental

Throughout the experiments, water was doubly distilled in an all-glass apparatus and the highest purity chemicals were used. The water was further boiled for 1 h and cooled under nitrogen (purified by a Sigma Oxiclear cartridge) in order to exclude $CO_2$ and $O_2$. The ionic strength was maintained constant with sodium perchlorate (Sigma). Perchloric acid (70%, Fluka) and sodium hydroxide (p.a., Merck) concentrations were determined, respectively, by the titration of sodium tetraborate solution (puriss. p.a., Fluka) in the presence of methyl red as indicator and potassium hydrogenphthalate (99.99%, Acros Organics) with phenolphthalein as indicator.

Investigated metalloporphyrin, MnTnBu-2-$PyPCl_5$ was synthesized according to published procedures [12]. Manganese(II) porphyrin was prepared by the reduction of manganese(III) porphyrin with ascorbic acid (Fluka), whereas the oxidation of manganese(III) porphyrin was performed by $K_3[Mo(CN)_8]$ that was prepared according to the published procedure [13, 14] immediately before the experiment. Concentration of $K_3[Mo(CN)_8]$ was determined spectrophotometrically ($\varepsilon_{388} = 1360\,(\text{mol L}^{-1})^{-1}\,\text{cm}^{-1}$) [15]. Both reduction and oxidation reactions were completely reversible, and the original manganese(III) porphyrin could be fully recovered by changing the ratio of reductant and oxidant or by changing the pH (*vide infra*).

A solution of $Mn^{III}$TnBu-2-$PyPCl_5$ ($\approx 4.0 \times 10^{-6}\,\text{mol L}^{-1}$) was prepared by the dilution of a stock solution in water. The ionic strength was adjusted with sodium perchlorate. Aliquots of 20 mL of this solution were introduced into a jacketed cell, maintained at $(25.0 \pm 0.2)^{\circ}$C. The free hydrogen ion concentration was measured with a combined glass electrode Mettler DG111-SC and Mettler T70 titrator. The Ag/AgCl reference electrode was filled with $3\,\text{mol L}^{-1}$ NaCl. The combined glass electrode was calibrated as a hydrogen concentration probe by titrating standard solution of $HClO_4$ with standard $CO_2$-free NaOH solution [16, 17].

The spectrophotometric titrations were carried out by the addition of aliquots of standardized NaOH solution with a piston microburet (Eppendorf). Special care was taken to ensure that complete equilibration was attained. Simultaneous p[$H^+$] and UV-Vis absorption spectra (350–600 nm) were recorded. Absorption spectra were recorded using a Varian Cary 50 UV-Vis spectrophotometer fitted with Cary 50 Fibre Optic Dip Probe Coupler.

Cyclic-voltammetry (CV) measurements were performed using a three-electrode potentiostat CH Instruments 600D, on-line connected to a PC. The data were treated by CHI software v9.23. The working, reference, and auxiliary electrodes were a glassy carbon (GC) electrode, the Ag/AgCl standard electrode ($3\,\text{mol L}^{-1}$ NaCl), and a platinum wire, respectively. GC electrode was polished with an aqueous alumina slurry with particles 0.05 μm in diameter before every experiment and the electrode surface was determined to be $0.08\,\text{cm}^2$ by chronocoulometry of 2 mM solution of $K_3[Fe(CN)_6]$ in $1\,\text{mol L}^{-1}$ aqueous KCl. The pH of aqueous solutions was determined on a Mettler Toledo T70 titrator with Mettler DG-111-SC glass electrode calibrated

Downloaded At: 07:10 23 January 2011

with standard pH 4.00, 7.00, and 10.00 buffers. The supporting electrolyte in CV measurements of manganese porphyrin was 0.1 mol $L^{-1}$ NaCl.

## 3. Results

### 3.1. *Spectrophotometric pH titration of MnTnBu-2-PyP complexes*

In aqueous solution, manganese porphyrins coordinate one or two axial waters, which depending on the pH could deprotonate according to reaction patterns (1)–(3).

$$(H_2O)_m Mn^X TnBu\text{-}2\text{-}PyP^n \rightleftarrows (HO)(H_2O)_{m-1} Mn^X TnBu\text{-}2\text{-}PyP^{(n-1)} + H^+ \quad (1)$$

$$(HO)(H_2O)_{m-1} Mn^X TnBu\text{-}2\text{-}PyP^{(n-1)} \rightleftarrows (O)(H_2O)_{m-1} Mn^X TnBu\text{-}2\text{-}PyP^{(n-2)} + H^+ \quad (2)$$

$$(O)(H_2O)_{m-1} Mn^X TnBu\text{-}2\text{-}PyP^{(n-2)} \rightleftarrows (HO)_2 Mn^X TnBu\text{-}2\text{-}PyP^{(n-2)} \quad (3)$$

In these equations $X$ and $n$ stand for oxidation numbers of manganese and the formal charges of the (di)aqua complexes, and $m$ is 1 or 2 depending on the oxidation state of manganese and/or degree of deprotonation, respectively.

Downloaded At: 07:10 23 January 2011

### 3.2. *Deprotonation of $Mn^{III}$TnBu-2-PyP*

As a representative example, the observed visible spectral change of the $Mn^{III}$TnBu-2-PyP in aqueous solution as a function of p[$H^+$] at $I = 2$ mol $L^{-1}$ is shown in figure 2.

Up to p[$H^+$] = 9, the absorption spectrum of $Mn^{III}$TnBu-2-PyP is characterized by an intense and sharp absorption centered at ~454 nm together with two weaker and broader absorption bands lying at 366 and 568 nm. The increase of p[$H^+$] induces a clear hypsochromic shift of the intense absorption band from 454 to 444 nm and the loss of the band at 366 nm. Absence of isosbestic points during the titration clearly indicates an involved equilibrium that includes several absorbing species. Spectral analysis using the SPECFIT program revealed three relevant absorbing species related by two mono-deprotonation processes. Fitting such a model to the experimental data at different ionic strengths resulted in the values of deprotonation constants given in table S1. Theoretical electronic spectra of different $Mn^{III}$TnBu-2-PyP species predicted from the fit are presented in the inset on figure 2.

Variations of the observed ionization constants of $Mn^{III}$TnBu-2-PyP with ionic strength and temperature are presented in figures 3 and 4, respectively.

Linear fit to the data shown in figure 3 resulted in the following parameters: (i) the first ionization constants; slope = 1.0 ± 0.1, intercept = 10.33 ± 0.07; (ii) the second ionization constants; slope = 1.1 ± 0.3, intercept = 11.2 ± 0.2. The obtained values of intercepts correspond to the first and second thermodynamic acidity constants of $(H_2O)_2Mn^{III}$TnBu-2-$PyP^{5+}$ calculated as $2.14 \times 10^{10}$ and $1.58 \times 10^{11}$ $dm^3$ $mol^{-1}$, respectively. From the intercepts and slopes of van't Hoff plots shown in figure 4, the reaction enthalpies and entropies were calculated as

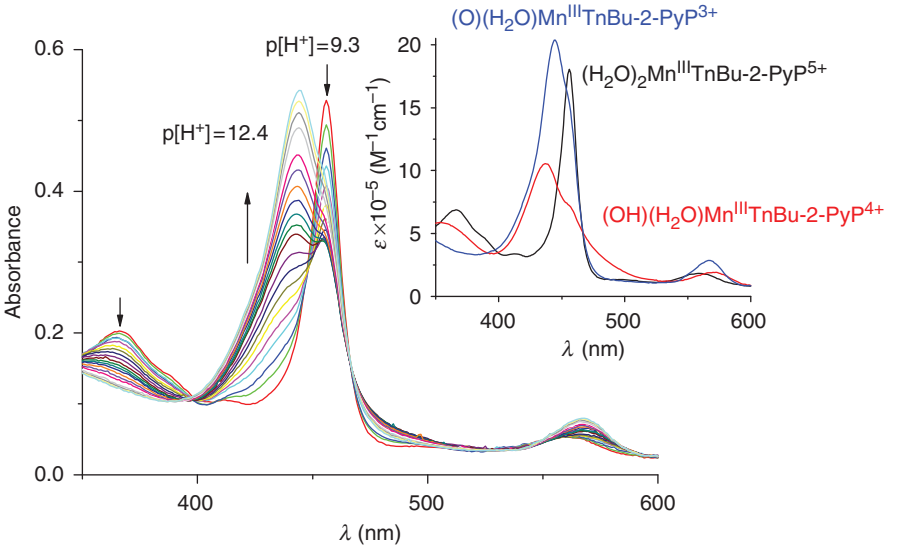


Figure 2. Spectrophotometric titration of $4 \times 10^{-6}$ mol L$^{-1}$ $Mn^{III}$TnBu-2-PyP with NaOH, $I = 2$ mol L$^{-1}$ ($NaClO_4$), $\theta = 25°C$, $l = 1$ cm. The p[$H^+$] values of the solution were varied within the p[$H^+$]-range 9.3–12.4 (for the sake of clarity not all the measured spectra are shown).

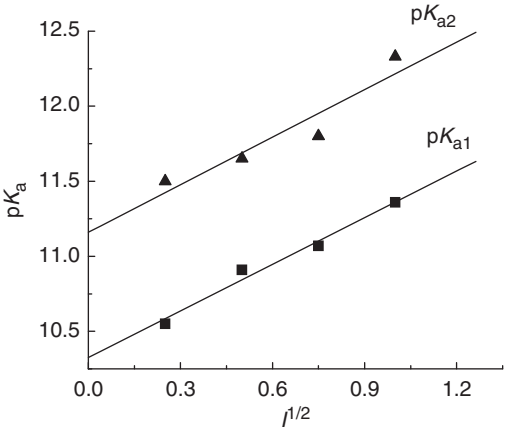


Figure 3. Dependence of p$K_a$s of $Mn^{III}$TnBu-2-PyP on $I^{1/2}$ at 25°C.

follows: $\Delta_{a1}H = 60 \pm 2$ kJ mol$^{-1}$, $\Delta_{a1}S = -16 \pm 8$ J K$^{-1}$ mol$^{-1}$, $\Delta_{a2}H = 49 \pm 4$ kJ mol$^{-1}$, and $\Delta_{a2}S = -67 \pm 8$ J K$^{-1}$ mol$^{-1}$.

### 3.3. *Deprotonation of $Mn^{II}$TnBu-2-PyP*

As a representative example, the observed visible spectral change of $Mn^{II}$TnBu-2-PyP in aqueous solution as a function of p[$H^+$] at $I = 2$ mol L$^{-1}$ is shown in figure 5.

Downloaded At: 07:10 23 January 2011

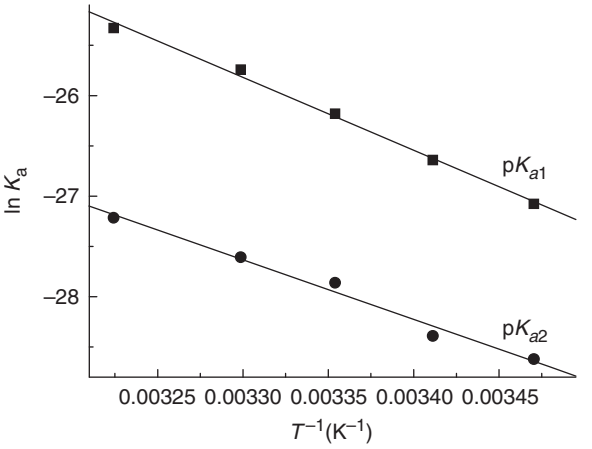


Figure 4. van't Hoff plots for the first and second ionization constants of $(H_2O)_2Mn^{III}TnBu\text{-}2\text{-}PyP^{5+}$ at $I = 2\,mol\,L^{-1}$ ($NaClO_4$).

Downloaded At: 07:10 23 January 2011

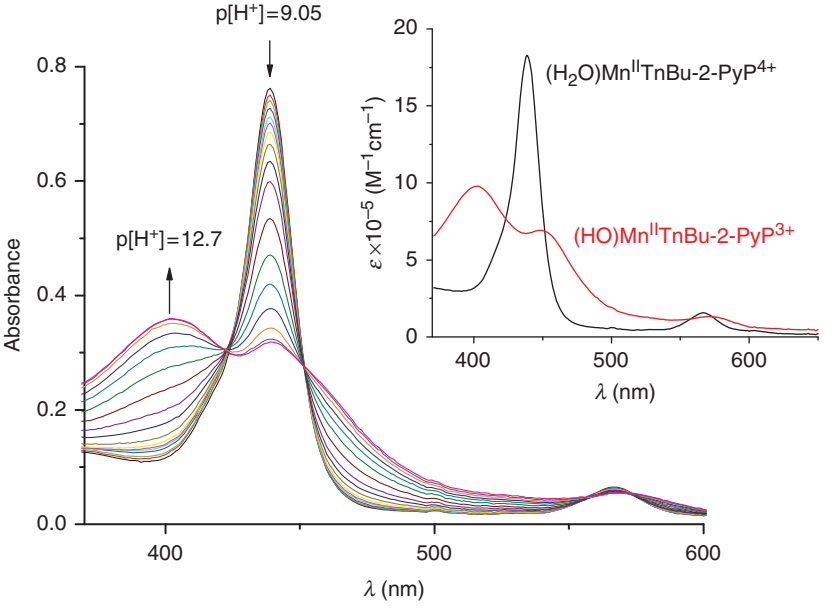


Figure 5. Spectrophotometric titration of $4\times10^{-6}\,mol\,L^{-1}$ $Mn^{II}TnBu\text{-}2\text{-}PyP$ with $0.2\,mol\,L^{-1}$ NaOH, in 10 mM ascorbic acid, $I = 2\,mol\,L^{-1}$ ($NaClO_4$), $\theta = 25°C$, $l = 1\,cm$. For the sake of clarity not all the measured spectra are shown.

The titration was carried out under purified nitrogen. Manganese ion in MnTnBu-2-PyP was maintained in reduced form by the addition of ascorbic acid in a large molar excess.

A slight shift of the isosbestic points observed during the titration could be indicative of an involved equilibrium. The SPECFIT factor analysis reveals at least two relevant absorbing species existing in solution, but the third one could not be

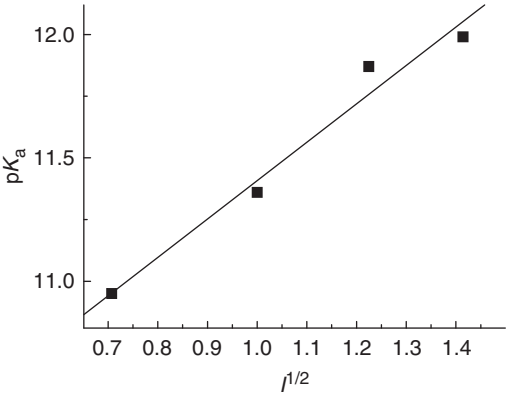


Figure 6. Dependence of p$K_a$ of $Mn^{II}$TnBu-2-PyP species on $I^{1/2}$ at 25°C.

Downloaded At: 07:10 23 January 2011

definitively discarded. Therefore, the observed spectral data were fitted to two different models, one affording two spectral species and one p$K_a$ value and another one affording three spectral species and two p$K_a$'s.

The three-species model for $Mn^{II}$TE-2-PyP deprotonation produces a slightly better fit, which can be expected due to more degrees of freedom. Judging from the standard deviations, that model is only slightly better than the two-species model and the residuals of spectral data are similar for both models. According to the three-species model, the first deprotonation of $(H_2O)Mn^{II}$TnBu-2-$PyP^{4+}$ causes an almost negligible hypsochromic shift of the spectrum, with the practically identical spectral shapes of diprotonated and monoprotonated species of $Mn^{II}$TnBu-2-PyP, differing only in their intensities. The calculated p$K_{a1}$ value has a 10-fold larger standard deviation than p$K_{a2}$, and the p$K_a$ value for the two-species model is remarkably similar to p$K_{a2}$ obtained from the three-species model. Therefore, the existence of the third spectral species could be just an artifact related to experimental errors and we assume with certainty only one p$K_a$ for acid–base equilibrium of $Mn^{II}$TnBu-2-PyP, whereas the other p$K_a$ cannot be confirmed with the current experimental data.

Accordingly, the two-species model was fitted to the observed spectral changes affording the calculation of the p$K_a$ values (table S2), and the electronic spectra for the different $Mn^{II}$TnBu-2-PyP species (inset of figure 5). The variations of the observed ionization constant of $Mn^{II}$TnBu-2-$PyP^{5+}$ with the ionic strength and temperature are presented in figures 6 and 7, respectively.

Linear fit to the data shown in figure 6 resulted in the following parameters: slope $= 1.5 \pm 0.2$, intercept $= 10.6 \pm 0.2$. The intercept corresponds to the thermodynamic acidity constant of $(H_2O)Mn^{II}$TnBu-2-$PyP^{4+}$ calculated as $3.98 \times 10^{10}$ $dm^3\,mol^{-1}$. From the intercept and slope of van't Hoff plot shown in figure 7, the reaction enthalpy and entropy were calculated as follows: $\Delta_{a1}H = 59 \pm 2\,kJ\,mol^{-1}$, $\Delta_{a1}S = -32 \pm 7\,J\,K^{-1}\,mol^{-1}$.

### 3.4. *Deprotonation of $Mn^{IV}$TnBu-2-PyP*

In order to determine the deprotonation patterns of the manganese(IV) porphyrins, the spectrophotometric titrations had to be performed in the presence of an

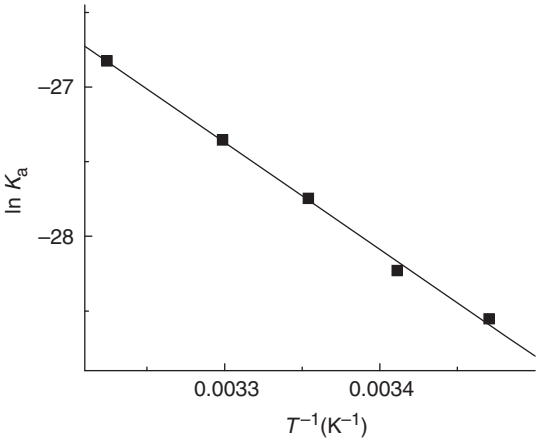


Figure 7. van't Hoff plot for acid dissociation of $Mn^{III}$TnBu-2-PyP at $I = 2\,mol\,L^{-1}$ ($NaClO_4$).

Downloaded At: 07:10 23 January 2011

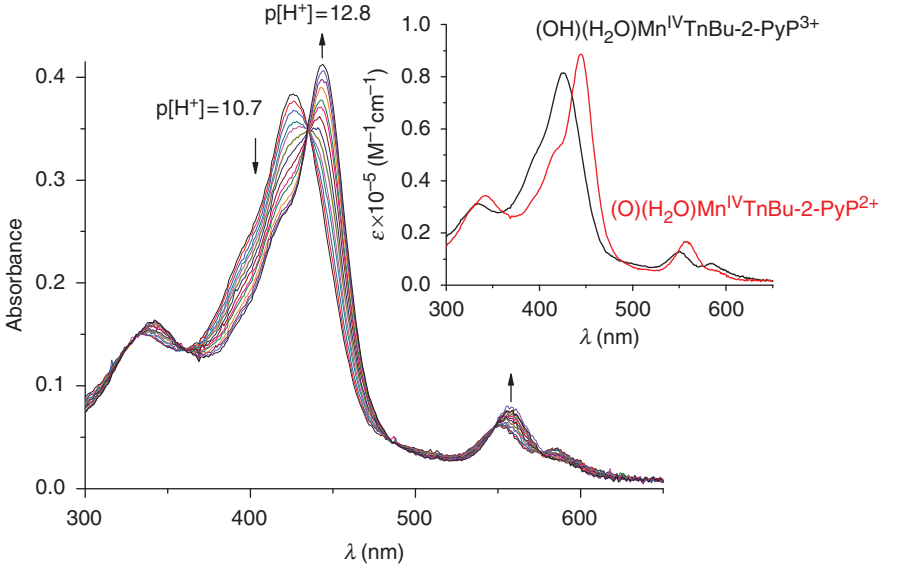


Figure 8. Spectrophotometric titration of $4 \times 10^{-6}\,mol\,L^{-1}$ $Mn^{IV}$TnBu-2-PyP with $0.2\,mol\,L^{-1}$ NaOH, $I = 2\,mol\,L^{-1}$ ($NaClO_4$), $\theta = 25°C$, $l = 1\,cm$. For the sake of clarity not all the measured spectra are shown.

efficient oxidant. Maintenance of MnTnBu-2-PyP in oxidized form was easily achieved by the addition of 0.1 mM $[Mo(CN)_8]^{3-}$, and by carrying out the pH titration in aqueous solution under purified argon. Dependence of the observed visible spectrum of the $Mn^{IV}$TnBu-2-PyP on pH in aqueous solution at $2\,mol\,L^{-1}$ ionic strength is shown in figure 8 as a representative example.

The spectral analysis using the SPECFIT program revealed two relevant absorbing species related through a single-proton exchange. Fitting such a model to the experimental data at different ionic strength resulted in the values of deprotonation

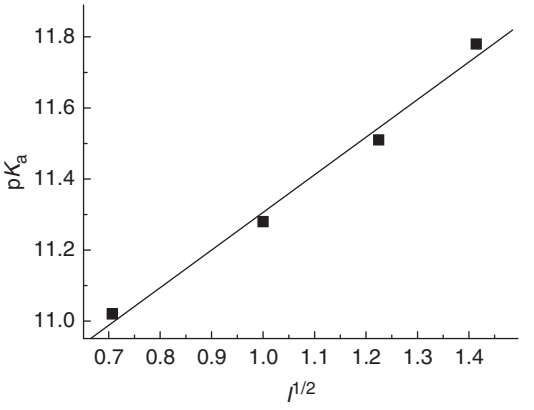


Figure 9. Dependence of $pK_a$ of $(H_2O)(OH)Mn^{IV}TnBu\text{-}2\text{-}PyP^{5+}$ on $I^{1/2}$ at 25°C.

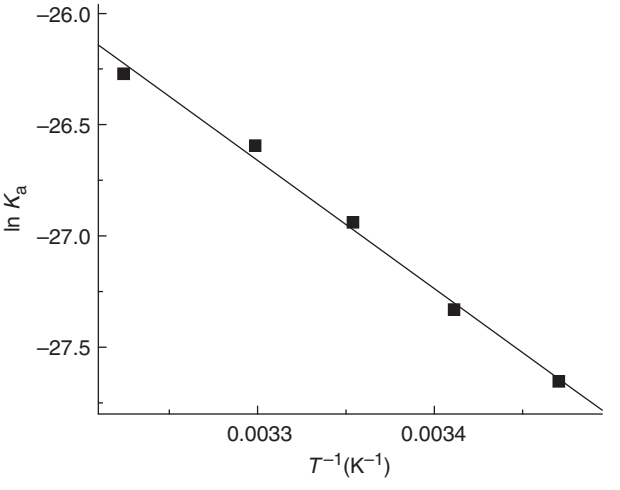


Figure 10. van't Hoff plot for $Mn^{IV}TnBu\text{-}2\text{-}PyP$ at $I = 2\,mol\,L^{-1}$ ($NaClO_4$).

constants given in table S3. The predicted theoretical spectral species are shown as inset in figure 8. Below pH 10 the Mn(III) form of complex ($Mn^{III}TnBu\text{-}2\text{-}PyP$) was extremely stable, hence any deprotonation constant were inaccessible by the present type of experiments. The variations of the observed ionization constants of $Mn^{IV}TnBu\text{-}2\text{-}PyP^{5+}$ with the ionic strength and temperature are presented in figures 9 and 10, respectively.

Linear fit to the data shown in figure 9 resulted in the following parameters: slope $= 1.06 \pm 0.08$, intercept $= 10.25 \pm 0.09$. The latter corresponds to $1.78 \times 10^{10}$ $dm^3\,mol^{-1}$ for the thermodynamic acidity constant of $(H_2O)(OH)Mn^{IV}TnBu\text{-}2\text{-}PyP^{5+}$. From the intercept and slope of the van't Hoff plot shown in figure 10, the reaction enthalpy and entropy were calculated as follows: $\Delta_{a1}H = 48 \pm 2\,kJ\,mol^{-1}$, $\Delta_{a1}S = -63 \pm 7\,J\,K^{-1}\,mol^{-1}$.

Downloaded At: 07:10 23 January 2011

### 3.5. *Cyclic voltammetry of MnTnBu-2-PyP*

In acidic and mildly basic media only one pH-independent current peak pair has been observed and attributed to Mn(III)/Mn(II) electron transfer (figure 11). At pH values above 9, an additional current peak pair appeared at more positive potentials, becoming fully developed at pH = 11, corresponding to the Mn(IV)/Mn(III) redox transition (figure 12). Cathodic ($E_{pc}$) and anodic ($E_{pa}$) peak separation for both redox processes increases with scan rate, $\nu$, indicative of a quasi-reversible single-electron transfer. Both potentials shift toward more negative values with increase in pH of the solution. Dependence of peak current, $i_p$, *versus* $\nu^{1/2}$ for the reduction of $Mn^{III}$TnBu-2-$PyP^{5+}$ (inset of figure 11), clearly demonstrates the transition from approximately reversible electron transfer at low values of $\nu$ to approximately irreversible electron transfer at high values of $\nu$. Similarly, peak currents of the Mn(III)/Mn(II) electron-transfer process measured at pH = 12 display even larger deviation from the reversible case, approximating to irreversible electron transfer at high values of $\nu$ (right-side inset of figure 12) [18].

Parameters of the recorded cyclic voltammograms were evaluated according to the previously published procedure [19, 20] and simulated using CHI software v9.23. A summary of the estimated electrochemical parameters for the Mn(III)/Mn(II) and Mn(IV)/Mn(III) redox couples is given in table 1. The data in table 1 are identical to the values of $E_{1/2}$ *versus* Ag/AgCl published previously [12], and the differences in potentials *versus* NHE are due to the differences in calibration. Yet, importantly, the

Downloaded At: 07:10 23 January 2011

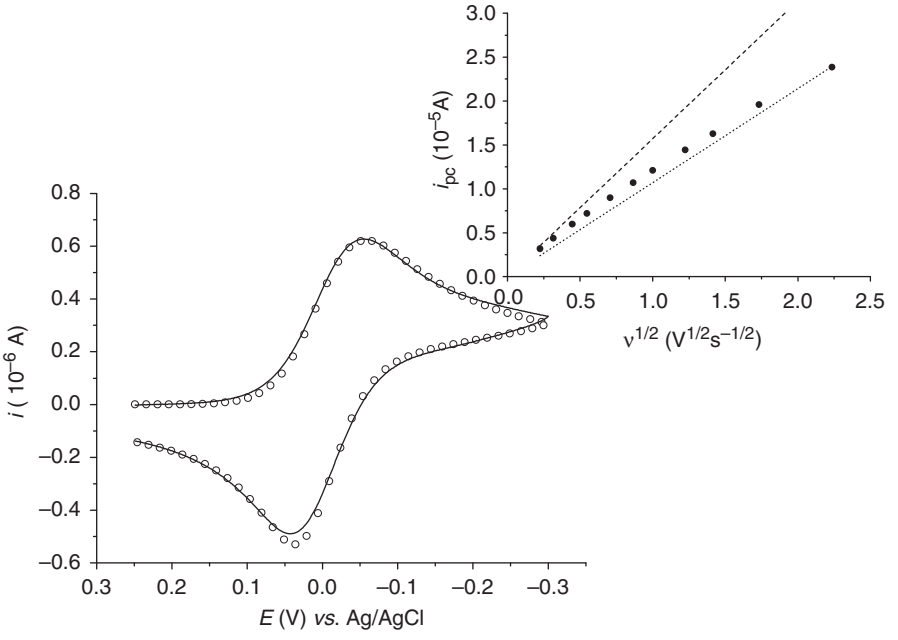


Figure 11. Cyclic voltammogram of $4.8 \times 10^{-4}$ mol $L^{-1}$ $Mn^{III}$TnBu-2-$PyP^{5+}$, pH = 7.6, $[NaH_2PO_4]$ = 0.05 mol $L^{-1}$, [NaCl] = 0.1 mol $L^{-1}$, $\nu = 0.2$ V $s^{-1}$, $\theta = 25°C$, (-) measured values, (○) simulated values. **Inset:** Dependence of $i_p$ on $\nu^{1/2}$, for the reduction of $Mn^{III}$TnBu-2-$PyP^{4+}$, (– –) Randles–Sevcik equation for reversible electron transfer, (· · ·) equation for irreversible electron transfer ($\alpha = 0.3$), (●) measured values of $i_{pc}$.

differences in potentials among the members of Mn(III) *N*-alkylpyridylporphyrin series hold and thus all relationships that have been based on $E_{1/2}$ hold also. Diffusion coefficients were obtained by chronoamperometry in the same cell.

The obtained results indicate a single-electron redox transition for the Mn(III)/Mn(II) redox couple, as defined by equation (4):

$$Mn^{III}TnBu\text{-}2\text{-}PyP(H_2O)_2^{5+} + e^- \rightleftarrows Mn^{II}TnBu\text{-}2\text{-}PyP(H_2O)^{4+} + H_2O \qquad (4)$$

The observed negative shift of the formal redox with increasing potential can be attributed to the above determined deprotonation equilibria of Mn(III) and Mn(II) species, in a way described by Laviron [21].

Deprotonation of these species also reduces the heterogeneous rate constant, probably caused by a decrease of the overall positive charge and formal reduction potential of the reacting species upon deprotonation. The value of cathodic electron-transfer coefficient $\alpha < 0.5$ is indicative of an asymmetric potential-energy function for the transition state, meaning that the structure of the activated complex of Mn(III)/Mn(II) redox couple has predominantly the structure of oxidized species. The literature data indicate that similar MnPs in the oxidized form, i.e., Mn(III), are six-coordinate

Downloaded At: 07:10 23 January 2011

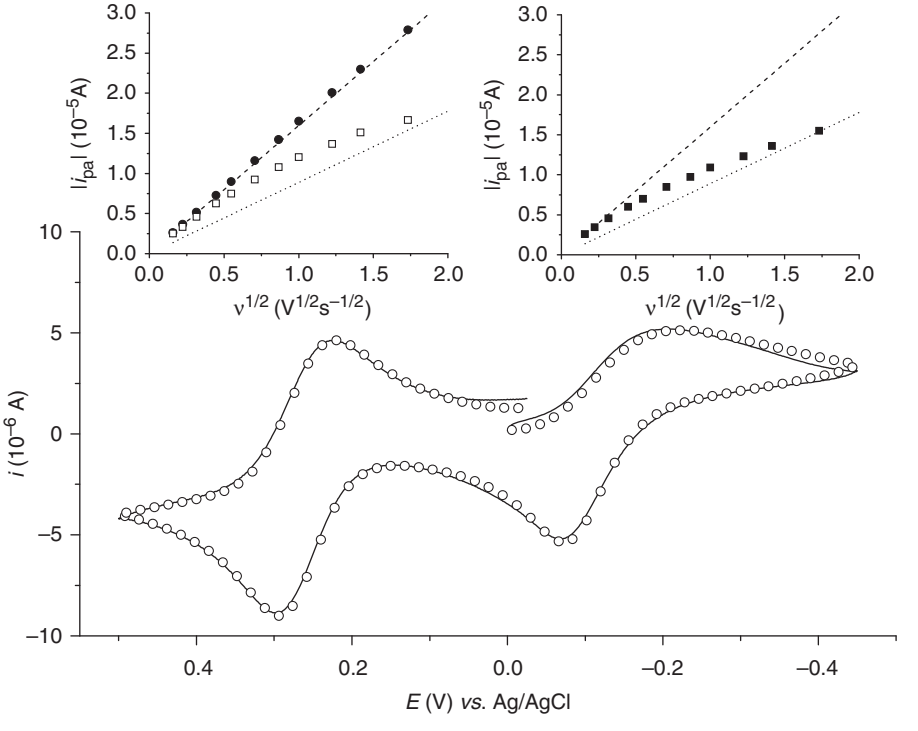


Figure 12. Cyclic voltammogram of $4.9 \times 10^{-4}$ mol $L^{-1}$ $Mn^{III}TnBu\text{-}2\text{-}PyP^{5+}$, pH = 12, $[Na_2HPO_4] = 0.05$ mol $L^{-1}$, [NaCl] = 0.1 mol $L^{-1}$, $\nu = 0.2$ V $s^{-1}$, $\theta = 25°C$, (-) measured values, (○) simulated values. **Left-side inset:** Dependence of $i_p$ on $\nu^{1/2}$, for the oxidation of $Mn^{III}TnBu\text{-}2\text{-}PyP^{5+}$, (––) Randles–Sevcik equation for reversible electron transfer, (●) measured values of $i_{pa}$, (···) equation for irreversible electron transfer ($\alpha = 0.2$), (□) measured values of $i_{pc}$. **Right-side inset:** Dependence of $i_p$ on $\nu^{1/2}$, for the oxidation of $Mn^{III}TnBu\text{-}2\text{-}PyP^{4+}$, (––) Randles–Sevcik equation for reversible electron transfer, (···) equation for irreversible electron transfer ($\alpha = 0.2$), (■) measured values of $i_{pa}$.

with distorted octahedral geometry whereas in the reduced form, i.e., Mn(II), are five-coordinate with geometry near a tetragonal pyramid [22]. The asymmetry of the potential-energy function is further increased upon deprotonation of the involved species ($\alpha = 0.3$ at pH = 7.6 and $\alpha = 0.2$ at pH 12).

The oxidation of Mn(III) to Mn(IV) species is hindered in acidic media. The absence of electrochemical response of the Mn(III)/Mn(IV) redox pair in acidic media is most likely due to oxo-/aqua-equilibrium of Mn(IV):

$$(H_2O)_2Mn^{IV}TnBu\text{-}2\text{-}PyP^{6+} \rightleftharpoons (H_2O)(O)Mn^{IV}TnBu\text{-}2\text{-}PyP^{4+} + 2H^+ \quad (5)$$

Whereas, the electrochemical reaction is limited to the oxo-complex making it thermodynamically unfavorable in acidic media. As the pH of the medium increases, the rate of electron transfer increases, resulting in fully developed anodic and cathodic waves at sufficiently high pH. However, this electron-transfer process is also characterized by asymmetric potential-energy function for the transition state ($\alpha = 0.2$). This asymmetry is further demonstrated by the observed peak current for the oxidation of $Mn^{III}TnBu\text{-}2\text{-}PyP^{5+}$ at pH = 12 matching the criteria of reversible electron transfer quite well, but this is not the case for the reduction of Mn(IV) species (left-side inset of figure 12).

Downloaded At: 07:10 23 January 2011

## 4. Discussion

The equilibrium spectrophotometric measurements reveal that within the studied acidity range three forms of $Mn^{III}TnBu\text{-}2\text{-}PyP$ and only two forms of $Mn^{IV}TnBu\text{-}2\text{-}PyP$ and $Mn^{II}TnBu\text{-}2\text{-}PyP$ could be identified in an aqueous solution with certainty. The assignments of these species to the deprotonation steps defined by equations (1)–(3) could be based on the effect of the charge of the central metal ion on the polarization of the O–H bond of the coordinated water. The higher the positive charge localized on the manganese ion, the lower is the $pK_a$ of the corresponding complex. Accordingly, it seems possible that for $Mn^{IV}TnBu\text{-}2\text{-}PyP$, the species that is missing is the fully protonated one, which could eventually exist at a much lower pH. However, as clearly shown by CV measurements presented in figure 11, due to its high reduction potential this complex species cannot be observed and studied by conventional techniques. On the other hand, for the $Mn^{II}TnBu\text{-}2\text{-}PyP$ the inaccessible species under the studied experimental conditions is probably the fully deprotonated one whose $pK_a$ is perhaps shifted to a much higher value due to the decrease of positive charge on the central manganese ion. This hypothesis is confirmed by the thermodynamic data shown in table 2. Deprotonation of the Mn(II) porphyrin complex is characterized by $59\,kJ\,mol^{-1}$ reaction enthalpy and $-32\,J\,K^{-1}\,mol^{-1}$ reaction entropy that closely resembles the values for the first deprotonation step of Mn(III) complex, whereas the deprotonation of the Mn(IV) porphyrin complex is characterized by $48\,kJ\,mol^{-1}$ reaction enthalpy and $-63\,J\,K^{-1}\,mol^{-1}$ reaction entropy that closely resembles the values for the second deprotonation step of Mn(III) complex. Furthermore, according to such an assignment of the deprotonation steps, the obtained first ionization constant for Mn(II) complex ($pK_a = 10.6$) is slightly larger than for Mn(III) complex ($pK_a = 10.3$), reflecting the stronger polarization of the O–H bond of coordinated water in the latter complex due

Table 1. Estimated electrochemical parameters for the Mn(III)/Mn(II) and Mn(IV)/Mn(III) redox couples of MnTnBu-2-PyP complex.

| | pH = 7.6 | pH = 12 | |
|---|---|---|---|
| Redox couple | Mn(III)/Mn(II) | Mn(III)/Mn(II) | Mn(IV)/Mn(III) |
| $E^{0'}$ (V) *vs.* NHE | 0.203 | 0.113 | 0.471 |
| $\alpha$ | 0.3 | 0.2 | 0.2 |
| $k^{\circ}$ (cm s$^{-1}$) | 0.004 | 0.0015 | 0.011 |
| $D_O$ (cm$^2$ s$^{-1}$) | $2.8 \times 10^{-6}$ | $2.8 \times 10^{-6}$ | $3.7 \times 10^{-6}$ |
| $D_R$ (cm$^2$ s$^{-1}$) | $2.6 \times 10^{-6}$ | $2.6 \times 10^{-6}$ | $2.8 \times 10^{-6}$ |

Conditions: $[NaH_2PO_4] = 0.05$ mol L$^{-1}$ or $[Na_2HPO_4] = 0.05$ mol L$^{-1}$, $[NaCl] = 0.1$ mol L$^{-1}$, $\theta = 25^{\circ}$C.

to its higher positive charge. In other words, $Mn^{III}$TnBu-2-PyP$^{5+}$, with the manganese in the Mn(III) form, is more electron deficient and binds axial water more strongly than the electron-rich reduced Mn(II) site in $Mn^{II}$TnBu-2-PyP$^{4+}$, making the water molecules in the former complex more acidic.

A decrease of *ca* 40 J K$^{-1}$ mol$^{-1}$ in reaction entropies from the first to the second deprotonation step is probably caused by the formation of oxo-manganese porphyrin complexes in the latter step, whose stronger hydration due to the increased dipole moments could decrease the reaction entropies. Such a hypothesis is also confirmed by CV measurements, namely, by the reduction of heterogeneous rate constant upon deprotonation of the Mn(III) species, from $k^{\circ} = 0.004$ cm s$^{-1}$ to $k^{\circ} = 0.0015$ cm s$^{-1}$ at pH 7.6 and 12 (table 1), respectively. The same situation is repeated in the second protonation step of the Mn(III) complex ($pK_a = 11.3$) compared to Mn(IV) complex ($pK_a = 10.3$), where a higher positive charge on manganese again causes a stronger polarization of O–H bond and in turn smaller $pK_a$ of Mn(IV) complex.

Our values of deprotonation equilibrium constants obtained for $Mn^{III}$TnBu-2-PyP favorably compare to values reported for the methyl analogue of the studied metalloporphyrin [23], i.e., $pK_{a1}$ ($Mn^{III}$TM-2-PyP) = 10.5, $pK_{a2}$ ($Mn^{III}$TM-2-PyP) = 11.4, and $pK_a$ ($Mn^{IV}$TM-2-PyP) = 10.5, additionally confirming the proposed assignment of deprotonation steps.

Substitution of butyl for methyl chains in the porphyrin ring does not change the acidity of coordinated water, although it was suggested that the core exposure in the *ortho*-manganese porphyrins is strongly affected by the length of the alkyl side chains [24]. A possible hindrance of coordinated water and a decrease in local dielectric constant caused by the alkyl chains, which may slow the rate of proton transfer between the axial ligand and the bulk water, must have a similar effect on both deprotonation and protonation rates of the complexes, causing no effect on the acid–base equilibria.

As shown in the distribution diagram (figure 13) of various species of MnTnBu-2-PyP calculated by use of the Hyss program [25], at pH 7.6 both Mn(II) and Mn(III) complexes are fully protonated, therefore the calculated formal reduction potential can be assigned to the couple $Mn^{III}$TnBu-2-PyP$(H_2O)_2^{5+}$/$Mn^{II}$TnBu-2-PyP$(H_2O)^{4+}$ ($E^{0'}$($Mn^{III}$TnBu-2-PyP$(H_2O)_2^{5+}$/$Mn^{II}$TnBu-2-PyP$(H_2O)^{4+}$) = +0.203 V *vs.* NHE).

From the determined values of deprotonation constants and the formal reduction potential for the aqua Mn(III)/Mn(II) porphyrin couple, the calculation of the formal potential for $Mn^{III}$TnBu-2-PyP$(H_2O)(OH)^{4+}$/$Mn^{II}$TnBu-2-PyP$(OH)^{3+}$ couple according to the Nernst equation yielded ($E^{0'}$($Mn^{III}$TnBu-2-PyP$(H_2O)(OH)^{4+}$/ $Mn^{II}$TnBu-2-PyP$(OH)^{3+}$) = +0.191 V *vs.* NHE). As expected, the calculated value

Downloaded At: 07:10 23 January 2011

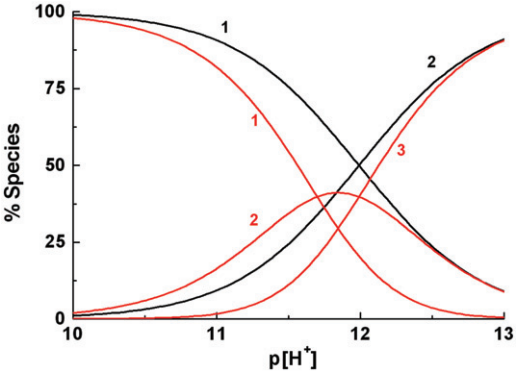


Figure 13. Distribution of MnTnBu-2-PyP species as function of pH at 25°C. Species: (**1**) $Mn^{III}$TnBu-2-PyP$(H_2O)_2^{5+}$, (**2**) $Mn^{III}$TnBu-2-PyP$(H_2O)(OH)^{4+}$, (**3**) $Mn^{III}$TnBu-2-PyP$(H_2O)=O^{3+}$; (**1**) $Mn^{II}$TnBu-2-PyP$(H_2O)^{4+}$ and (**2**) $Mn^{II}$TnBu-2-PyP$(OH)^{3+}$.

Downloaded At: 07:10 23 January 2011

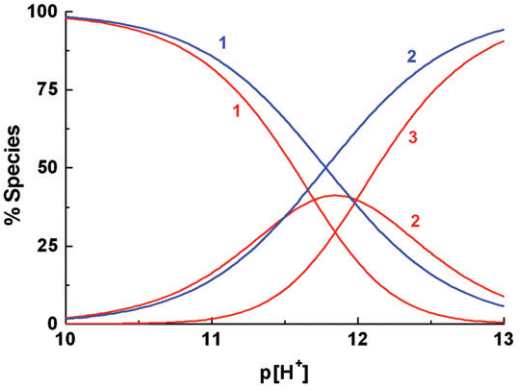


Figure 14. Distribution of MnTnBu-2-PyP species as function of pH at 25°C. Species: (**1**) $Mn^{III}$TnBu-2-PyP$(H_2O)_2^{5+}$, (**2**) $Mn^{III}$TnBu-2-PyP$(H_2O)(OH)^{4+}$, (**3**) $Mn^{III}$TnBu-2-PyP$(H_2O)=O^{3+}$; (**1**) $Mn^{IV}$TnBu-2-PyP$(H_2O)(OH)^{5+}$ and (**2**) $Mn^{IV}$TnBu-2-PyP$(H_2O)=O^{4+}$.

demonstrates that upon deprotonation of Mn(III) and Mn(II) aqua porphyrin complexes, the electron density on Mn(III) is slightly increased over Mn(II) central ion. As the presence of the oxo-complex was not confirmed for the Mn(II) complex, analogous comparison for this type of complex is impossible.

From figure 13 it is obvious that at pH 12, in both the oxidized and reduced form of the porphyrin complex, no complex species dominates in solution. Therefore, reduction potential in that solution was calculated using the appropriate form of Nernst equation. The estimated formal potential of 0.129 V *versus* NHE is in good agreement with the observed value at that pH listed in table 1, i.e., 0.113 V *versus* NHE indicating a reliability of the results obtained by two techniques used throughout this study.

A similar analysis can be performed for the reduction of Mn(IV)/Mn(III) studied complex. Figure 14 shows that at pH 10 two species dominate, the diaqua complex of Mn(III)-porphyrin complex and hydroxo complex of the Mn(IV) species. Therefore, the formal reduction potential, $E^{0'}=0.62$ V *versus* NHE, obtained by CV measurements at

Table 2. Equilibrium parameters for the deprotonation of MnTnBu-2-PyP of various oxidation states of central metal ion.

| Manganese oxidation state in MnTnBu-2-PyP | First deprotonation | | | Second deprotonation | | |
|---|---|---|---|---|---|---|
| | $pK_{al}$[a] (25°C) | $\Delta H_a$ ($kJ\,mol^{-1}$) | $\Delta S_a$ ($J\,K^{-1}\,mol^{-1}$) | $pK_{a2}$[a] (25°C) | $\Delta H_a$ ($kJ\,mol^{-1}$) | $\Delta S_a$ ($J\,K^{-1}\,mol^{-1}$) |
| Mn(II) | $10.6 \pm 0.2$ | $59 \pm 2$ | $-32 \pm 7$ | | | |
| Mn(III) | $10.3 \pm 0.1$ | $60 \pm 2$ | $-16 \pm 8$ | $11.2 \pm 0.2$ | $49 \pm 3$ | $-67 \pm 8$ |
| Mn(IV) | | | | $10.3 \pm 0.1$ | $48 \pm 2$ | $-63 \pm 7$ |

[a]At $I = 0$, obtained from the intercept of the "$pK_a$ *vs.* $I^{1/2}$" plots.

pH 10, mainly corresponds to the $Mn^{IV}$TnBu-2-PyP$(H_2O)(OH)^{5+}$/$Mn^{III}$TnBu-2-PyP$(H_2O)_2^{5+}$ couple, described by the half-reaction: $Mn^{IV}$TnBu-2-PyP$(H_2O)(OH)^{5+} + H^+ + e^- \rightarrow Mn^{III}$TnBu-2-PyP$(H_2O)_2^{5+}$.

At pH 12 there is no the oxidized or reduced MnP species that dominates the solution and the equilibrium appears to be too much involved to permit calculation of any particular formal reduction potential. However, combining the obtained value of $E^{0'}(Mn^{IV}$TnBu-2-PyP$(H_2O)(OH)^{5+}/Mn^{III}$TnBu-2-PyP$(H_2O)_2^{5+})$ with the $pK_a$ values from table 2 yielded the formal reduction potential of *ca* 0.58 V at pH = 12 for any hypothetical value of the first deprotonation constant of the Mn(IV) species $pK_{a1} < 9.5$. It is unlikely that the $pK_{a1}$ is higher than 9.5 because the third absorbing species, $Mn^{IV}$TnBu-2-PyP$(H_2O)_2^{6+}$, should have been observed in the spectrophotometric titrations. The calculated formal reduction potential is significantly different from the observed formal potential of 0.471 V *versus* NHE, indicating that equation (5) might indeed be significant at lower pH values.

In conclusion, our results confirm that the fully deprotonated $Mn^{II}$TnBu-2-PyP$(=O)^{2+}$ species does not exist in a basic water solution up to pH 13. On the other hand, based on the obtained results the $Mn^{IV}$TnBu-2-PyP inaccessible species could not be specified with certainty. It could be the fully protonated one, but because of the possible formation of $Mn^{IV}$TnBu-2-PyP$(H_2O)(=O)^{4+}$ in a double-deprotonation step from $Mn^{III}$TnBu-2-PyP$(H_2O)_2^{5+}$ the inaccessible species could also be the fully deprotonated oxo-complex. Therefore, further studies including other MnP analogues should be undertaken in order to clarify this point.

Downloaded At: 07:10 23 January 2011

## Acknowledgments

The authors are thankful to the Croatian Ministry of Science (MZOŠ grant: 006-0061247-0009) and to Duke University's CTSA grant 1 UL 1 RR024128-01 from NCRR/NIH for their financial support.

## References

[1] I. Batinić-Haberle, J.S. Reboucas, I. Spasojević. *Antioxid. Redox Signal*, (2010). DOI: 0.1089/ars.2009.2876.
[2] D. Salvemini, S. Cuzzocrea. *Crit. Care Med.*, **31**, S29 (2003).
[3] C. Szabó, H. Ischiropoulos, R. Radi. *Nat. Rev. Drug Discovery*, **6**, 662 (2007).

[4] I. Spasojević, Y. Chen, T.J. Noel, Y. Yu, M.P. Cole, L. Zhang, Y. Zhao, D.K. St Clair, I. Batinić-Haberle. *Free Radical Biol. Med.*, **42**, 1193 (2007).
[5] I. Batinić-Haberle, I. Spasojević, R.D. Stevens, B. Bondurant, A. Okado-Matsumoto, I. Fridovich, Z. Vujasković, M.W. Dewhirst. *J. Chem. Soc., Dalton Trans.*, 617 (2006).
[6] I. Spasojević, I. Batinić-Haberle, J.S. Rebouças, Y.M. Idemori, I. Fridovich. *J. Biol. Chem.*, **278**, 6831 (2003).
[7] I. Batinić-Haberle, L. Benov, I. Spasojević, P. Hambright, A.L. Crumbliss, I. Fridovich. *Inorg. Chem.*, **38**, 4011 (1999).
[8] H. Saba, I. Batinić-Haberle, S. Munusamy, T. Mitchell, C. Lichti, J. Megyesi, L.A. MacMillan-Crow. *Free Radical Biol. Med.*, **42**, 1571 (2007).
[9] Y. Zhao, L. Chaiswing, T.D. Oberley, I. Batinić-Haberle, W. St Clair, C.J. Epstein, D. St Clair. *Cancer Res.*, **65**, 1401 (2005).
[10] I. Batinić-Haberle, M.M. Ndengele, S. Cuzzocrea, J.S. Rebouças, I. Spasojević, D. Salvemini. *Free Radical Biol. Med.*, **46**, 212 (2009).
[11] I. Kos, J.S. Rebouças, G. DeFreitas-Silva, D. Salvemini, Ž. Vujasković, M.W. Dewhirst, I. Spasojević, I. Batinić-Haberle. *Free Radical Biol. Med.*, **47**, 72 (2009).
[12] I. Batinić-Haberle, I. Spasojević, R.D. Stevens, P. Hambright, I. Fridovich. *J. Chem. Soc., Dalton Trans.*, 2689 (2002).
[13] J.G. Leipoldt, L.D.C. Bok, P.J. Cilliers, Z. Anorg. *Allg. Chem.*, **409**, 343 (1974).
[14] R.W. Bucknall, W. Wardlaw. *J. Chem. Soc.*, 2981 (1927).
[15] G.W. Gray, J.T. Spence. *Inorg. Chem.*, **10**, 2751 (2002).
[16] P. Gans, B. O'Sullivan. *Talanta*, **51**, 33 (2000).
[17] A.E. Martell, R.J. Motekaitis. *Determination and Use of Stability Constants*, VCH, Weinheim (1988).
[18] D.T. Sawyer, A. Sobkowiak, J.L. Roberts. *Electrochemistry for Chemists*, 2nd Edn, John Wiley & Sons, Inc, New York (1995).
[19] R.S. Nicholson, I. Shain. *Anal. Chem.*, **36**, 706 (1964).
[20] H.J. Paul, J. Leddy. *Anal. Chem.*, **67**, 1661 (1995).
[21] E. Laviron, J. Electroanal. *Chem.*, **146**, 15 (1983).
[22] A. Harriman, G. Porter. *J. Chem. Soc., Faraday Trans.*, **2**, 1532 (1979).
[23] F.C. Chen, S.H. Cheng, C.H. Yu, M.H. Liu, Y. Oliver Su. *J. Electroanal. Chem.*, **474**, 52 (1999).
[24] R.W. Wagner, T.E. Johnson, J.S. Lindsey. *J. Am. Chem. Soc.*, **118**, 11166 (1996).
[25] L. Alderighi, P. Gans, A. Ienco, D. Peters, A. Sabatini, A. Vacca. *Coord. Chem. Rev.*, **184**, 311 (1999).

Downloaded At: 07:10 23 January 2011